6. FATIGUE ASSESSMENT AND CORRELATION

6.1 SCOPE

There are in essence two methods which could be used to substantiate the results obtained in the previous chapter. Firstly, as the major aim of the design and testing requirements is to ensure that real operational loading conditions are accurately simulated, it is possible to verify such results by applying them to predict or reproduce failures that have been experienced in the field.

Secondly, the results can be compared to requirements set in design standards.

In this chapter, failure predictions and comparisons with actual failures experienced on the case study vehicles, or similar/older models, are dealt with. Comparison with design code loads are also described.

The chapter also contains a section dealing with a method to derive input loading from field failure data, without the need for measurements and surveys, that was developed during the minibus case study. This method is presented here since it is an inverse of the method to predict failures.

6.2 FATIGUE LIFE PREDICTION

6.2.1 General

Failure predictions and comparison with actual field failures are described for every case study.

6.2.2 Minibus

6.2.2.1 Method

To verify the theoretical distributions obtained from the measurements and questionnaires, it was attempted to use these distributions to obtain a theoretical prediction of the failures that had occurred in practice on the crossmembers. A methodology was subsequently developed to predict the failures that would have occurred before a certain reference date ($date_{ref}$), the result of which could then be compared to actual failure data on that date.

In paragraph 5.5.3 the average damage to failure (D_f) of the crossmember was based on the laboratory test results. A vehicle that was sold in a certain month would be on the road for a certain number of days (assumed 22 working days per month) up to $date_{ref}$. By dividing D_f by the number of days, a constant number for each month results:

$$constant_{month} = D_f \text{ / days on the road} \qquad \textbf{Eq. 6-1}$$

This constant then implies a hyperbola for each month on the D/km, km/day plane, since:

$$D/km \times km/day = D/day = constant_{month} \qquad \textbf{Eq. 6-2}$$

The probability that a vehicle that has been sold during a certain month preceding $date_{ref}$ would have failed before $date_{ref}$ can then be calculated by calculating the volume above

the hyperbola on the D/km, km/day plane and underneath the surface described by the fitted 2-D PDF. This volume can be calculated by double integration as follows:

$$P_{month} = \int_{x1=0}^{\infty} \int_{x2=\frac{constant_{month}}{x_1}}^{\infty} f(x_1, x_2)\, dx_2\, dx_1$$

$$\text{with } f(x_1, x_2) = \text{as defined by Eq. 5 - 33}$$

$$x_1 = \text{D/km}$$

$$x_2 = \text{km/day}$$

$$P_{month} = \text{probability that a vehicle sold in certain month will fail before data}_{ref}$$

$$constant_{month} = \text{as defined by Eq. } 6-2$$

Eq. 6-3

This process is graphically depicted in Figure 6-1, which depicts a contour plot of the 2-D PDF together with the hyperbolas for incremental age (only month=1 and month=2 are tagged, but the hyperbolas to the left are for one month increments up to month=9). The contour plot is essentially a top view of Figure 5-26. The contours represent constant values of probability density.

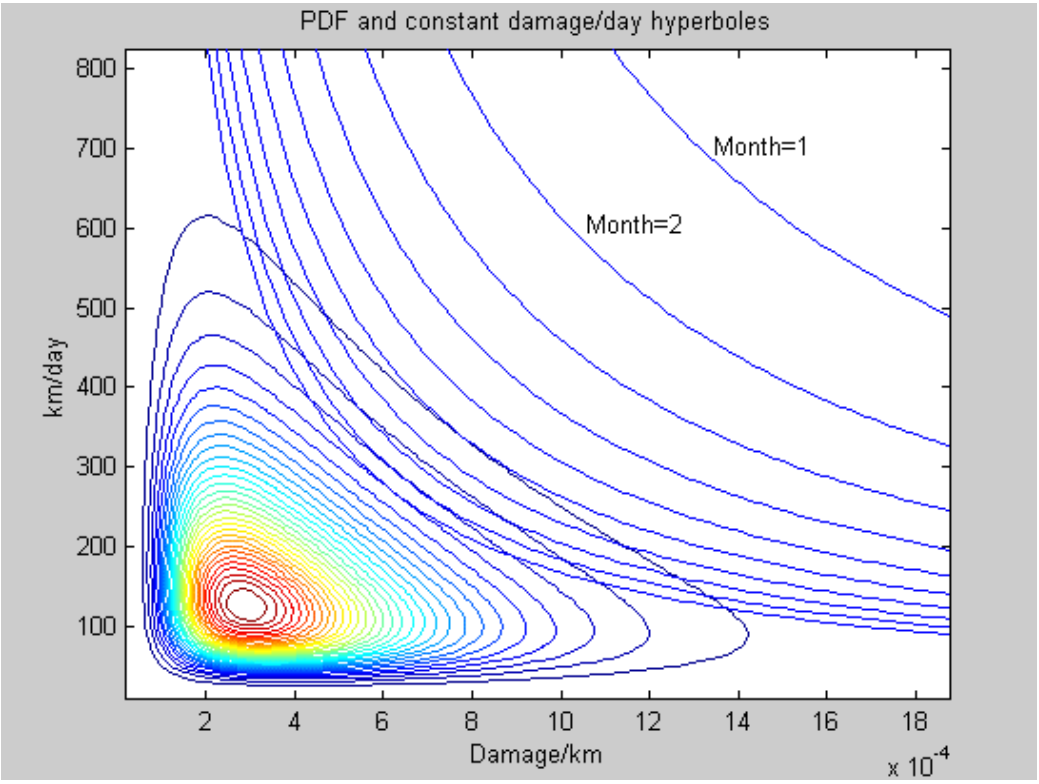

Figure 6-1 Integration of PDF

The total number of vehicles predicted to have failed by $date_{ref}$ may then be calculated as follows:

$$\text{Predicted number of failures} = \sum_{month=1}^{date_{ref}} \left(P_{month} \, sales_{month} \right)$$

Eq. 6-4

The distribution of distance to failure of the vehicles predicted to have failed can also be determined by calculating the number of vehicles for all months for each increment of x_1 (dam/km) which would have failed:

$$N(x_1) = \sum_{month=1}^{day_{ref}} \left[\left(\int_{x2=\frac{constant_{month}}{x_1}}^{\infty} f(x_1, x_2)\, dx_2 \right) \Delta x_1 \times sales_{month} \right]$$

$$\text{with } f(x_1, x_2) = \text{as defined by Eq. 5 - 33}$$

$$x_1 = \text{D/km, being incremented from } \Delta x_1 \text{ to } \infty \text{ in steps of } \Delta x_1$$

$$x_2 = \text{km/day}$$

$$N(x_1) = \text{number of vehicles predicted to have failed after } \frac{D_f}{x_1} \text{ kilometres}$$

$$constant_{month} = \text{as defined by Eq. } 6-3$$

Eq. 6-5

6.2.2.2 Testing

6.2.2.2.1 Test method

A test rig was erected which was able to simulate the relevant loads acting on the crossmember. The test rig consisted of three servo-hydraulic actuators. Two actuators were employed to simulate the vertical front wheel displacements and a third actuator was used to simulate the vertical inertial forces due to the gearbox acting on the crossmember. The test rig configuration is depicted in Figure 6-2.

Three signals measured on the test track were used as control signals, namely:

- Strain gauge on left torsion bar measuring torsional shear strains, used to control the left wheel actuator.
- Strain gauge on right torsion bar, measuring torsional shear strains, used to control the right wheel actuator.
- Strain gauge on gearbox mounting bracket, measuring strains caused by vertical inertial forces, used to control the gearbox actuator.

Drive signals for the three actuators were computed, using time domain based identification software, to accurately simulate the measured signals.

Three specimens were tested to failure. Failure was assumed to have occurred as soon as a crack developed in the crossmember.

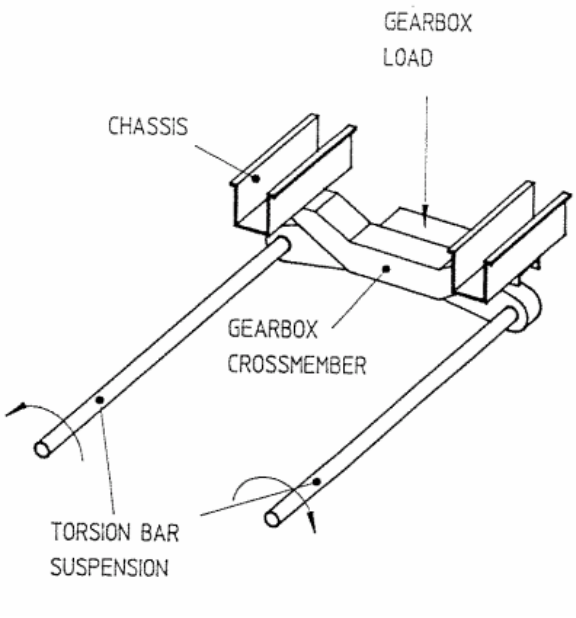

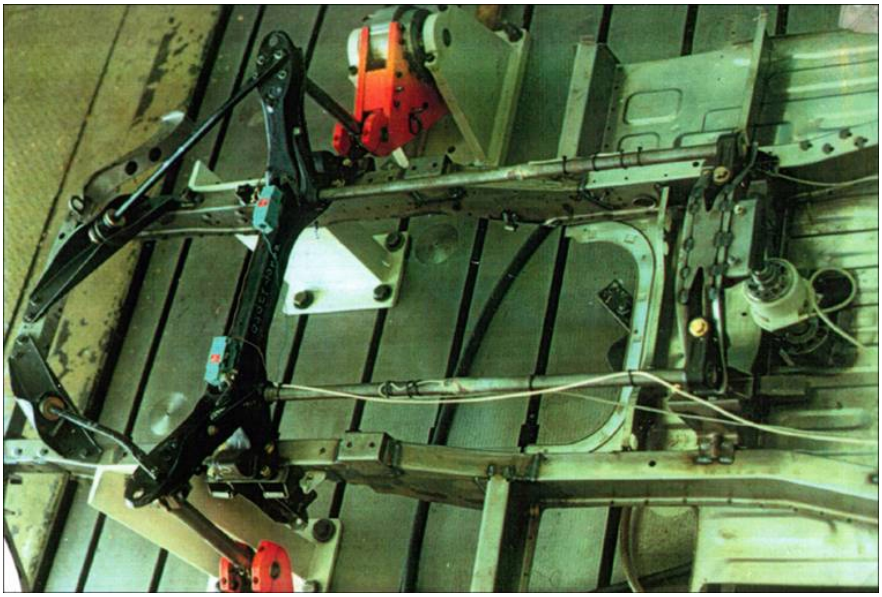

Figure 6-2: Test rig

6.2.2.2.2 Test results

The following number of test track cycles to failure was recorded for the three specimens that were tested:

Specimen no. 1:	1040 cycles	⇒ 26.87 relative damage
Specimen no. 2:	860 cycles	⇒ 22.22 relative damage
Specimen no. 3:	1240 cycles	⇒ 32.04 relative damage
Average :	1047 cycles	⇒ 27.06 relative damage

All cracks developed in the same position as had the field failures and there could be little doubt that the loading conditions had been the same. Some scatter was observed. It was

not possible to take account of this scatter in a statistical manner since too few specimens were tested. In subsequent analyses, the average damage to failure was therefore used.

6.2.2.3 Sales data

The specific minibus model was introduced to the market in December 1989. The sales for each month up to February 1991 (chosen as $date_{ref}$), are listed in Table 6-1.

Table 6-1 Sales figures for minibus

Month/Year	Sales	Month/Year	Sales
12/89	61	7/90	291
1/90	181	8/90	345
2/90	191	9/90	184
3/90	277	10/90	178
4/90	265	11/90	147
5/90	239	12/90	75
6/90	335	1/91	44

6.2.2.4 Results

The prediction calculations were subsequently performed using the theoretical distributions. The number of vehicles predicted to have failed was found to be more than the actual number of failures that had occurred up to February 1991 (308 vs 44).

Several reasons for this discrepancy could be put forward:

- The measurements were performed on a fully laden vehicle. Since it is probable that a certain portion of the distance reported by each participant would be travelled with an empty or half laden vehicle, the damage per kilometre would be overestimated.
- The questionnaire exercise may have been biased in relation to the total population of taxi operators. The number of participants may have been too small to obtain representative results. Also, the exercise involved only certain regions. Also it is not certain whether the percentages and distances per day quoted by the participants are applicable to 100 % of the distance covered by the vehicles and every day of the week. One participant quoted that he travels 1600 km/day, which seems unrealistic as an average distance per day. A better result would have been obtained if the average distance travelled per month had been asked.
- The damage to failure determined through laboratory testing was defined at the observance of a visible crack. Field failures may only have been reported after the crack had almost severed the crossmember. It was not possible to simulate this in the laboratory since the test had been performed in displacement control and not load control, implying that the induced force would diminish as the crossmember looses stiffness due to crack growth. The damage to failure may therefore have been underestimated by an unknown margin. This would cause an overestimation of the number of failures. A further test was subsequently performed on a cracked specimen to quantify this factor. The drive signals for the actuators were adjusted during the test to take account of the loss of stiffness of the specimen as the crack progressed, thus keeping the load inputs constant. The test was performed until final failure. A further 728 cycles resulted, implying that the damage to failure should be increased by a factor of 1.7.

- The number of sold vehicles utilized as taxis was unknown. It was assumed that 100% of the total sales had been utilized as taxis. An over estimation of the number of sales applicable to operational taxis (and therefore to the theoretical distributions) would cause an over estimation of the number of failures.
- Failures occurring in the field may not all have been reported.

It was not possible to quantify all of the above factors. A sensitivity study was however performed to study the influence of each factor on the prediction results. Adjustment factors were introduced within estimated reasonable ranges until a close correspondence between the actual failure results and the predicted results were obtained. The following factors were introduced:

- The damage per kilometre data was divided by a factor of 1.4.
- The kilometre per day data was divided by a factor of 1.8.
- The average number of operational days per month was taken as 20.
- The damage to failure was multiplied by a factor of 1.7, following the extended laboratory test.
- The number of vehicles utilized as taxis was taken as 0.6 times the total number sold.
- The number of failures reported was taken as 0.6 times the total number of failures.

The above set of adjustment factors does not represent a unique solution for obtaining a close correspondence between the prediction and the actual failure results, but was so chosen so as to result in a conservative estimation of the operational conditions pertaining to taxi vehicles.

The above process resulted in 45 vehicles being predicted to have failed in comparison to the actual 44. More importantly, however, is the good correspondence between the predicted and actual distributions of distance to failure. This comparison is shown in Figure 6-3. This result implied that the calibrated calculation process proved to be very successful.

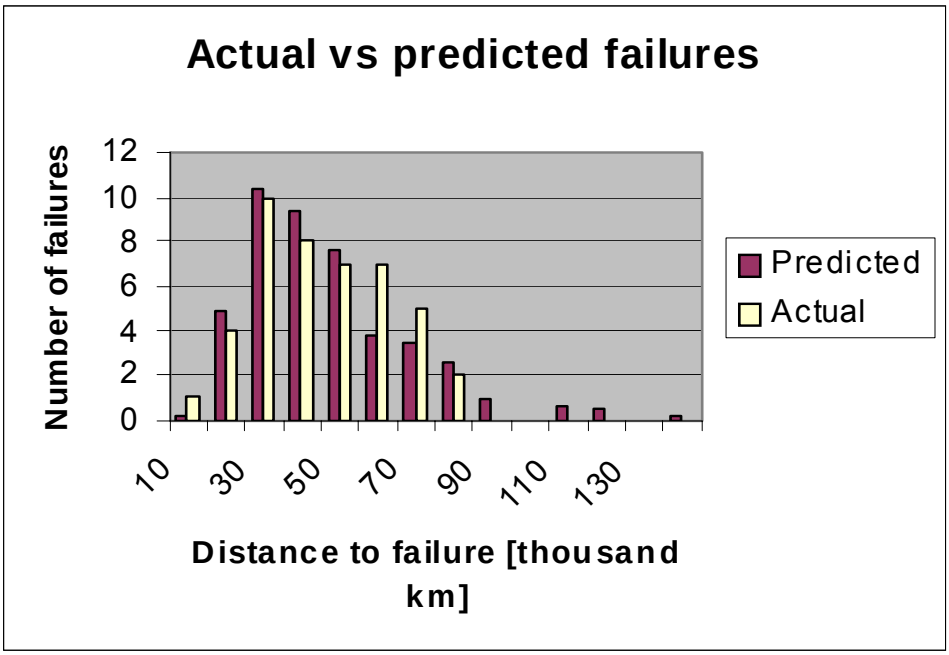

Figure 6-3 Actual vs predicted failures for minibus crossmember

6.2.2.5 Monte Carlo simulation

An alternative approach to the analytical approach used above for the prediction of failures, is the Monte Carlo simulation method discussed by Slavik and Wannenburg. The advantage of this approach is that it enables expansion of the number of variables treated as statistical variables. The Monte Carlo simulation method was applied to the pick-up truck case study, as described in paragraphs 5.5.4, 5.6.3 and 6.2.3. For the pick-up truck, no actual failure data was available and therefore the application of the method to the minibus case study, where correlation with actual failures can be demonstrated, serves as verification of the method.

As explained before and applied to the minibus, the method creates a large number of vehicles and randomly assigns to each one a D/km and a km/month parameter, such that the bivariate distribution of these two parameters for the created population, closely corresponds to the distribution derived above from the measurements and surveys. This is achieved through the process depicted in Figure 5-32.

It is then a simple matter to calculate the distance to failure (D_f / damage per km) and the months to failure (distance to failure / km per month) for each random vehicle. These results, together with the actual sales data, are used to predict the failure rates. The result of this analysis is depicted in Figure 6-4.

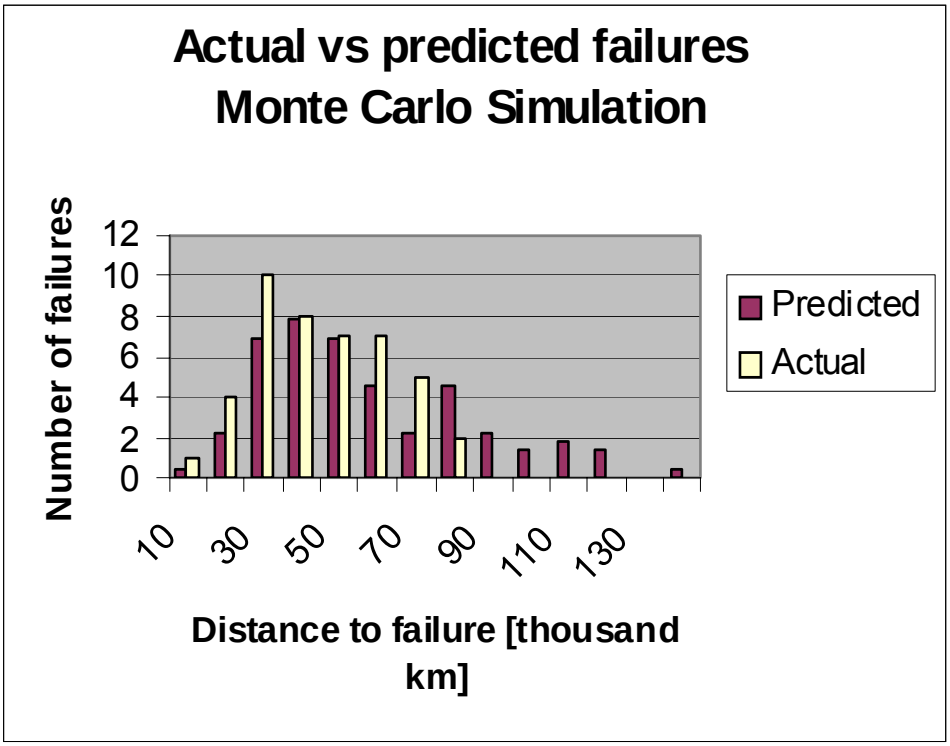

Figure 6-4 Actual vs Monte Carlo predicted failures for minibus crossmember

The results are similar to the results achieved with the analytical approach, as it should be, and therefore verifies the Monte Carlo approach.

6.2.2.6 Summary

A methodology has been developed to establish durability qualification test requirements for minibus vehicles based on South African conditions. The investigation involved a

statistical and fatigue representation of the operational conditions pertaining to taxi vehicles, based on the results of extensive measurements of road conditions, as well as data obtained from a questionnaire.

The theoretical results were used to predict the failures of gearbox mounting crossmembers that had failed in practice. The predicted results were compared to the actual failure results and with some adjustments, excellent correspondence was achieved. Durability requirements were subsequently derived.

The process thus established proved to be extremely successful. It is proposed that the methodology could be generalized to be applicable to any vehicle and could be used to address the establishment of durability test requirements in a powerful scientific manner.

A reverse method, based on the above is presented in paragraph 6.4 to derive a statistical representation of the usage profile of a vehicle in terms of fatigue damage, based only on failure data and sales data, without the use of questionnaires.

6.2.3 Pick-up Truck

6.2.3.1 Objectives

It was required to qualify the vehicle for South African conditions, which was to be defined by the usage profile exercise. It was aimed to perform the test for a sufficient duration such that all failures that may be expected to occur in the customer fleet within a reasonable life of the vehicle, would be reproduced on the test rig. The target was set as the equivalent of 300 000 km of 95 % of all users.

6.2.3.2 Laboratory test rig

The test rig consisted of four vertical servo-hydraulic actuators, with two 40kN actuators for the front wheels and two 100kN actuators for the rear wheels. (Dissimilar actuators were used simply due to equipment availability). Each actuator was equipped with a horizontal wheel platform that was provided with a mechanism preventing rotation of the actuator ram about the vertical axis. Restriction of fore-aft movement of the vehicle was provided by a small round bar at the front and rear of each of the front wheels, while lateral movement of the vehicle was prevented by side plates on the outsides of the four wheels on the wheel platforms. An axial fan with blow tubes was used as cooling aid for the vehicle's shock absorbers. The actuators were driven in displacement command mode and controlled via a digital to analogue interface system from a PC.

The test vehicle was placed on its wheels on the four poster road simulator. No side forces, braking or acceleration forces were therefore simulated. From previous experience, it is argued that a large portion of structural damage induced on pick-up truck vehicles would be caused by vertical inputs, since it is a vehicle intended to be used for carrying cargo on often rough road surfaces.

The test vehicle was fully laden since the field data sections used were all for the fully laden condition.

6.2.3.3 Calculation of actuator drive signals

It was necessary to perform two separate drive signal calculations. Low frequency drive signals were calculated from response data measured by the coil spring strain gauges and the differential strain gauges, filtered to contain frequencies between 0 and 5 Hz

only. High frequency drive signals were calculated from response data measured from the wheel accelerations, filtered to contain frequencies between 5 and 25 Hz (the accelerometers, although necessary to measure the high frequency inputs, do not respond at the low frequencies). The two drive signals were then superimposed to obtain the final drive signal.

The process to derive drive signals for the test rig is described in paragraph 3.4.6.2.

Due to hydraulic limitations, as well as safety considerations, it was not possible to achieve the same acceleration factors for the rear wheels to those achieved for the front wheels.

6.2.3.4 Relation between laboratory durability sequence and usage profile distance

The same fatigue damage calculation procedure was applied to the test rig measured responses for all the strain gauges. This resulted in the fatigue damage induced by the road simulator during one cycle of the laboratory test sequence.

The results are listed in Table 6-2. Again, comparison of the values for different channels has no meaning.

From this information, the required number of cycles to achieve the target test distance, pertaining to the 95 % user, could be determined, as described in paragraph 5.6.3.2.

Table 6-2 Test damage per cycle

Strain channel	Description	Test D/cycle $\times 10^{-6}$
1	Left front coil spring	179.3
2	Right front coil spring	261
3	Right rear differential	79
4	Left rear differential	6.5
5	Left front strut	1.1
6	Right front beam outside	111.4
7	Left beam centre between wheels	14.7
8	Round cross member	0.9
9	Left top door corner	1.6
10	Loadbox left rear panel	0

Although the intention was to achieve an equal acceleration for all channels, this was not achieved. The differences between the front wheel and rear wheel channels were ascribed to hydraulic limitations. The relatively low kilometre value of channel 10 could be attributed to the fact that a canopy that was fitted during the field measurements to protect the equipment, was not fixed onto the loadbox during the durability test. It is argued that a canopy changes the stiffness characteristics of the loadbox and hence affects the damage/kilometre results.

The test was terminated before achieving the target distance, due to failures.

6.2.3.5 Road simulator test failure results

When evaluating the test failure results, every failure can be related to one of the measurement channels by assessing which load input would primarily be causing the failure. All the failure events together with their corresponding cycles and damages to failure and assigned strain channel(s) are listed in Table 6-3.

Table 6-3 Road simulator test results

Damage	Cycles	Event	Corresponding Strain channel(s)
0.0024	302	Left rear leaf spring failure	3,4
0.0044	557	Right rear leaf spring failure	3,4
0.0033	416	Left rear leaf spring failure	3,4

The failures occurred well before the required 2000 cycles. The average cycles to failure was 425 and from Figure 5-34 it can be seen that this implies 300 000 km for the average (50 %) user.

6.2.3.6 Fatigue life prediction

Using the failure results, it was possible to perform a statistical failure prediction calculation. The first step was to use Bayesian inference to derive the statistical properties of the failure results. For this a prior mean and standard deviation had to be chosen, assuming a log-normal distribution. The posterior distribution was then derived from the combination of the prior distribution and the real failure results. The results of this calculation are depicted in Figure 6-5. A significantly smaller standard deviation was chosen for the prior distribution, but the relatively wide ranging failure results, implied a posterior distribution with a larger spread.

The Monte Carlo simulation method then requires a random failure damage (D_f) to be chosen according to the above distribution, for each of the 10 000 samples of x_1 (km/month) and x_2 (D/km) chosen using the process depicted in Figure 5-32.

The months to failure for each random sample (i) can then be calculated:

$$\text{months to failure}_i = D_{fi} / (x_{1i} \times x_{2i})$$

The results are then sorted from small to large and plotted against each sample's index (i) /1000 $\times$ 100, to yield a cumulative distribution of months to failure against cumulative percentage user, as depicted in Figure 6-6. The months to failure predicted for an improved design of the leaf springs which would survive the required 2000 test cycles can be calculated and similarly plotted:

$$\text{months to failure}_i = \text{D per cycle} \times 2000 / (x_{1i} \times x_{2i})$$

The distance to failure is calculated and plotted in Figure 6-7;

$$\text{distance to failure}_i = D_{fi} / x_{2i}$$

and for an improved design:

$$\text{distance to failure}_i = \text{D / cycle} / x_{2i}$$

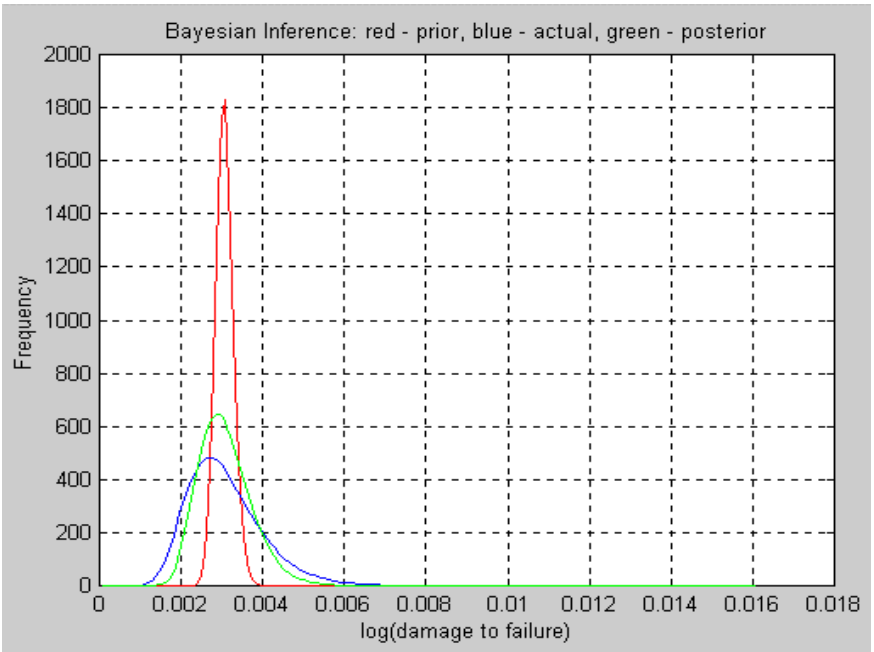

Figure 6-5 Bayesian inference of pickup truck damage to failure

From these graphs it can be seen that with the current design, 33 % of users will experience failures within 5 years (60 months) and 50 % will experience failure before 300 000 km. With the improved design, less than 3 % will experience failures within 5 years and less than 5 % before 300 000 km (as was intended).

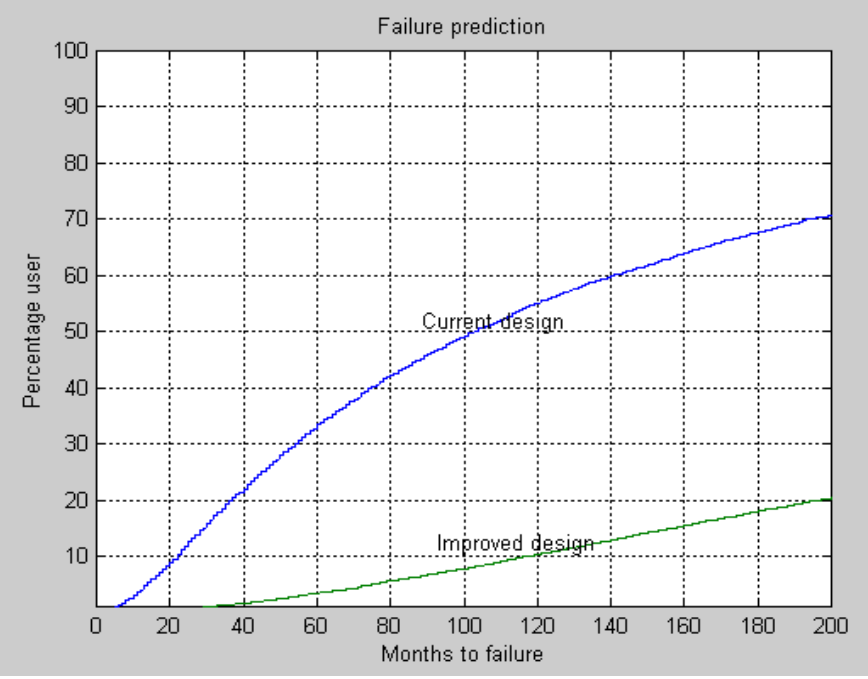

Figure 6-6 Time-to-failure prediction for pickup truck

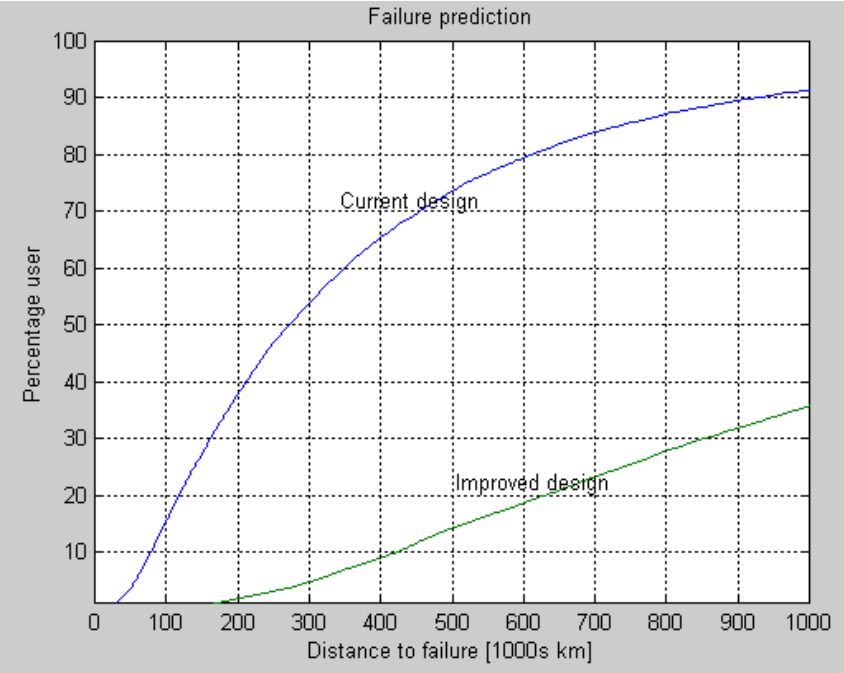

Figure 6-7 Distance-to-failure prediction for pickup truck

6.2.4 Fuel Tanker

6.2.4.1 Fatigue life prediction of prototype design

The fuel tanker design process described thus far, included comprehensive measurements on a prototype vehicle, based on which fatigue design criteria were derived (see paragraph 5.4.4). These criteria were subsequently used to estimate the fatigue life of the prototype design, according to the method described in paragraph 5.4.2.1.5. It was found that acceptable lives were estimated for all critical areas, except for a bulkhead support beam, the design of which therefore had to be modified. It was therefore expected to have no failures during the required life of the vehicles of 2 million kilometres. The majority of the fleet has to date exceeded the required life and in most cases no structural failures have been reported, thereby substantiating the FESL process. Premature field failures had been however reported on some vehicles, which were then investigated, as described in the following paragraphs.

6.2.4.2 Field failure description

The failures occurred on vehicles that were fitted with underslung axles, which were introduced due to availability problems with the overslung axles that were used in the original design. The engineering change procedure failed to highlight the fact that a large access hole (refer to Figure 6-8) for the airbag was to be introduced on the inside of the lower flange of the chassis beam in a critical stress area. The cracks experienced in the field all originated from this hole (after typically 800 000 km) and in some cases propagated into the web to almost sever the beam.

6.2.4.3 Prediction of field failures

6.2.4.3.1 Finite element analysis

The complete half model of the front trailer was used for the analysis (refer to paragraph 5.4.4.1). The access hole was modeled and the mesh was refined in the critical area. Vertical inertial loading was applied.

The stresses at the hole for a 1 g vertical loading are depicted in Figure 6-9. A maximum peak stress of 114 MPa is observed at the side of the hole.

6.2.4.3.2 Fatigue assessment

The fatigue design criterion established in paragraph 5.4.4.3 was that a fatigue life of 2 million kilometres on the vehicle is represented by 2 million cycles of a vertical loading range of 0.62 g. The fatigue equivalent peak stress range ($\Delta\sigma_e$) at the side of the access hole, to be experienced 2 million times during a 2 million kilometre life, would therefore be:

$$\Delta\sigma_e = 0.62 \times 114 = 71 \text{ MPa}$$

The material SN-curve for unwelded Aluminum in BS 8118 (1991) has a class of 60 (2.3% probability of failure), implying a fatigue strength (stress range) of 60 MPa at 2 million cycles.

The corresponding material fatigue properties as per Eq. 3-14 may be calculated as follows:

$$\Delta\sigma = S_f N^b$$
$$b = -0.333$$
$$\therefore 60 = S_f \left(2 \times 10^6\right)^{-0.333}$$
$$\therefore S_f = 7\,523 \text{ MPa}$$

The life to failure implied by the 71 MPa applied peak stress range can then be calculated:

$$\Delta\sigma = S_f N^b$$
$$\therefore N = \left(\frac{\Delta\sigma}{S_f}\right)^{1/b}$$
$$\therefore N = \left(\frac{71}{7523}\right)^{1/-0.333} = 1.2 \times 10^6 \text{ cycles}$$

Since 2 million cycles represents 2 million kilometres :

Predicted distance to failure $= 1.2 \times 10^6$ km

The predicted life correlates very well with the field failures, therefore again powerfully verifying the FESL method.

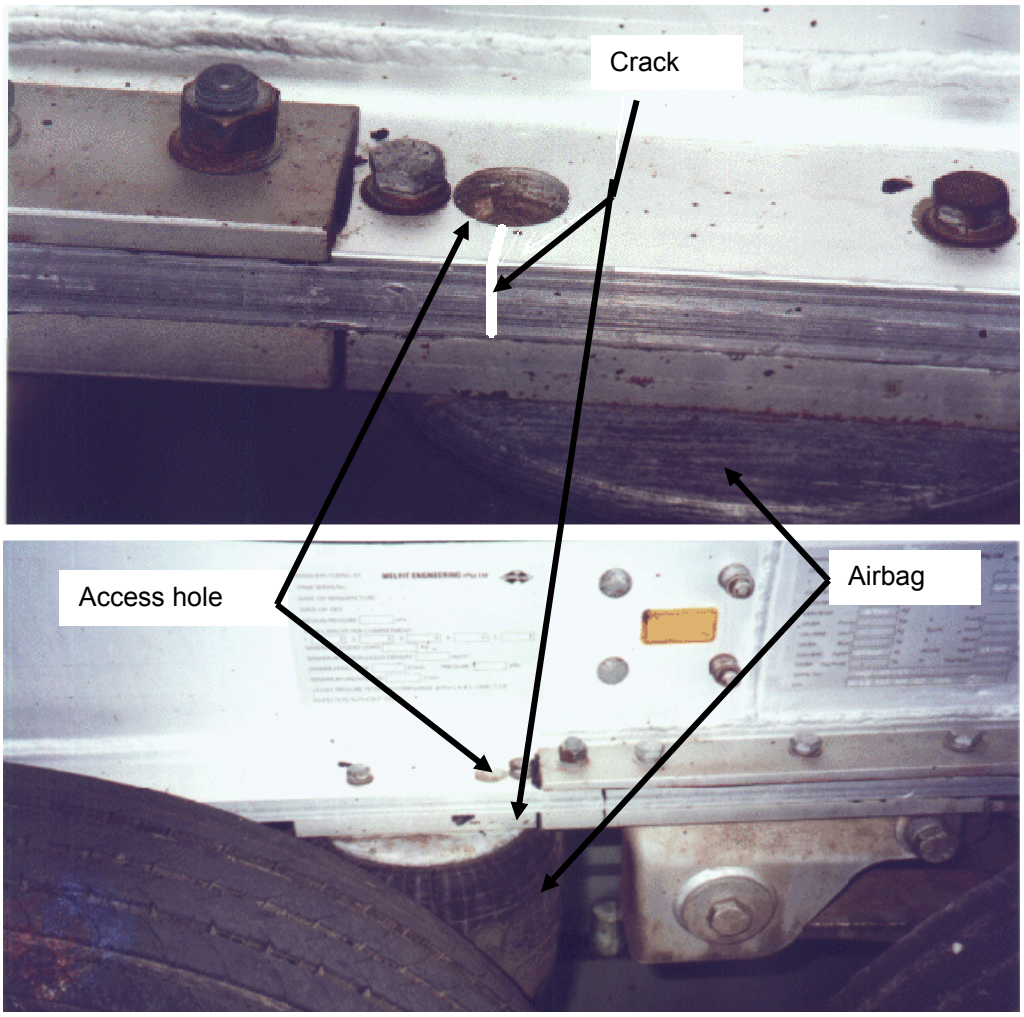

Figure 6-8 Field failure on fuel tanker

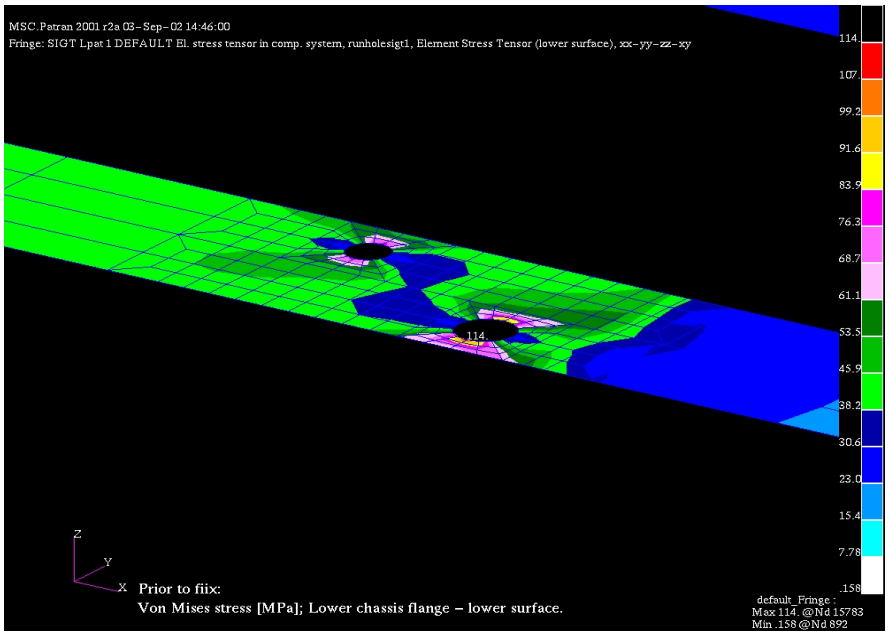

Figure 6-9 Fuel tanker chassis flange stresses

6.2.5 Ladle Transport Vehicle

6.2.5.1 Fatigue life prediction

The fatigue life estimation was performed using the Fatigue Module (based on nCode algorithms) of the MSC Patran software. The time histories of the vertical and lateral g-loads, as well as the modal participation factor (derived in paragraph 5.3.2.1), are multiplied separately with the unit load finite element stress results, obtaining stress histories for the total model. These stress histories are then superimposed to give total stress-time histories for the total model. Prescribing then the relevant SN material properties and understanding that the time histories would be repeated (80 000 hours / duration of histories in hours) times for a life, the hours to failure are calculated for the total model, based conservatively on the maximum absolute principal stresses. The software package performs the rainflow cycle counting and damage calculations internally and outputs contour plots of hours-to-failure.

6.2.5.2 Results

Some typical results are depicted in Figure 6-10 to Figure 6-13. Problem areas are pointed out with numbered arrows:

1) Web stresses perpendicular to cross member to web fillet weld.
2) Bottom flange stresses perpendicular to doubler plate fillet welds.
3) Top flange stresses perpendicular to doubler plate fillet wells.

Based on the above results, modifications were designed to achieve acceptable lives in the problem areas.

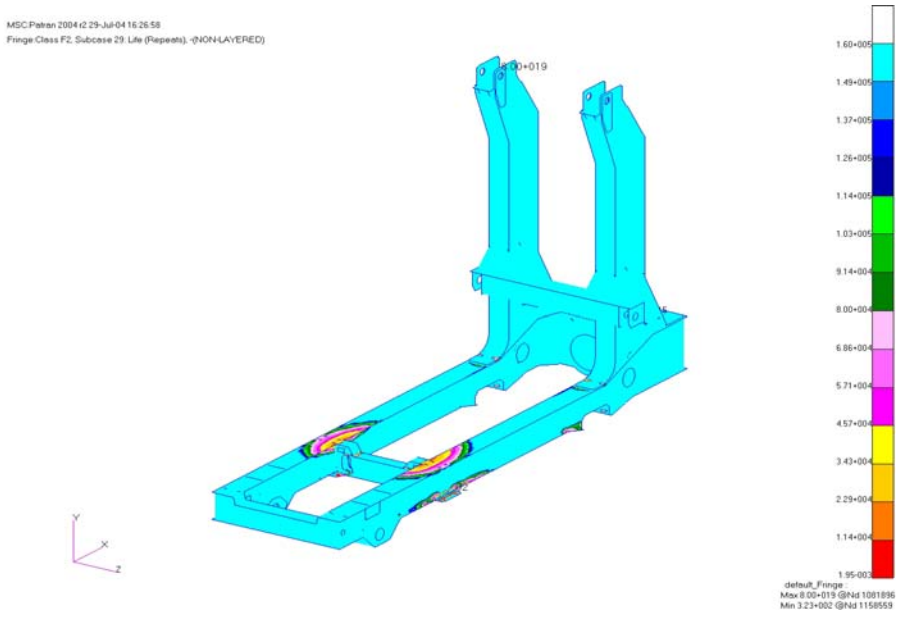

Figure 6-10 Estimated fatigue life for total model

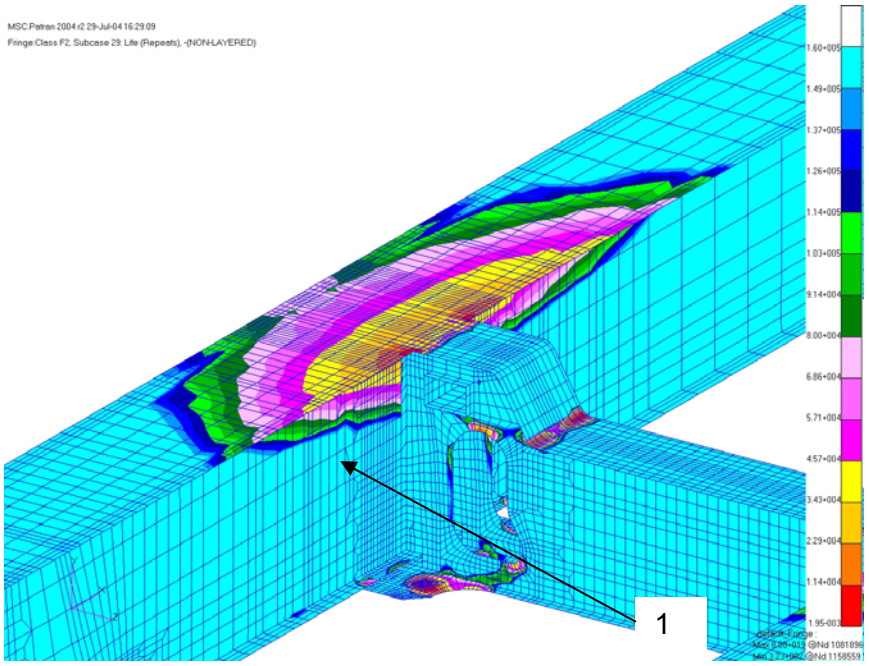

Figure 6-11 Fatigue life for crossmember to chassis welds

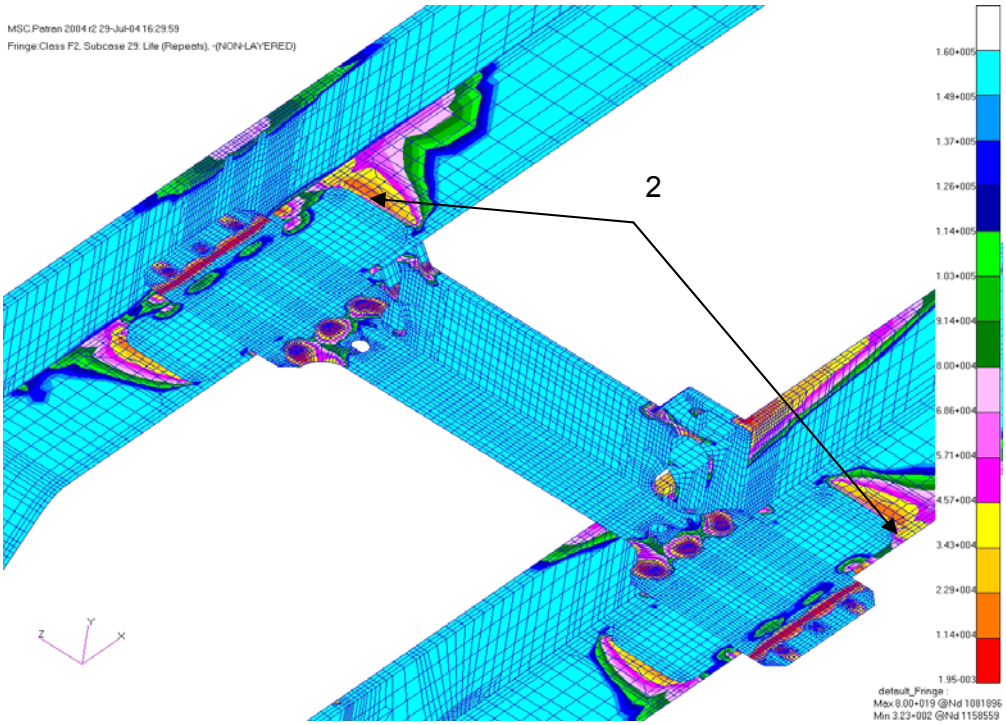

Figure 6-12 Fatigue life for doubler plate welds

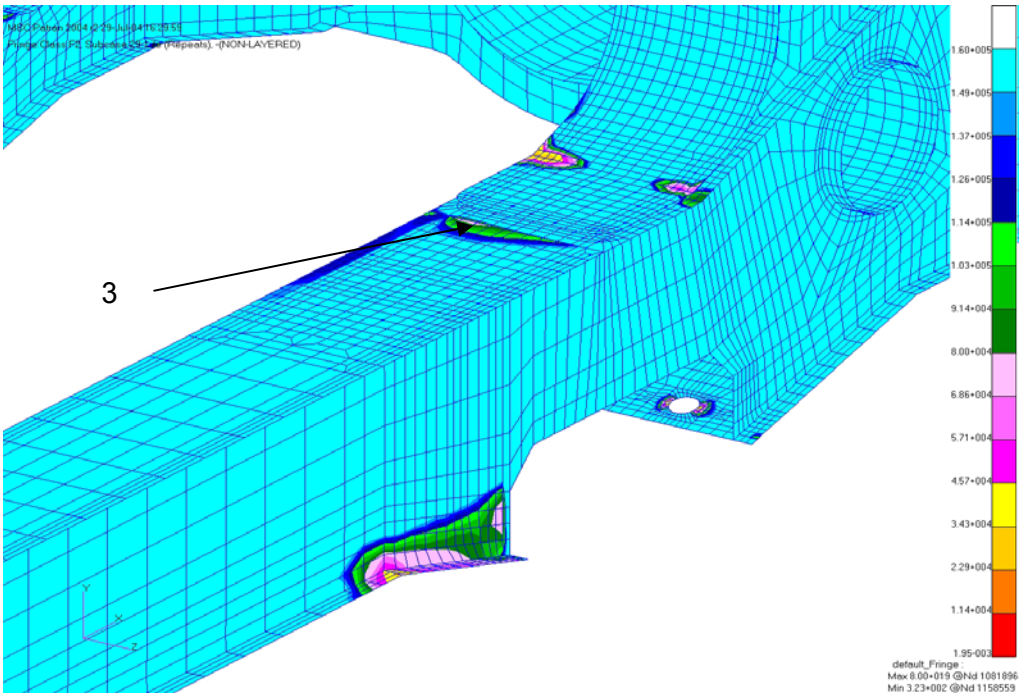

Figure 6-13. Fatigue life for chassis to pillar doubler plate welds

6.2.6 Load Haul Dumper

6.2.6.1 Fatigue life prediction

All the critical connections in the vehicle structure in the finite element model were divided into different groups, which correspond with the categories described in BS 7608 (1993). The parent metal, for example, was grouped as a category C, and a full penetration fillet weld as a category D, etc. The weld categories as chosen for the vehicle are depicted in Figure 6-14.

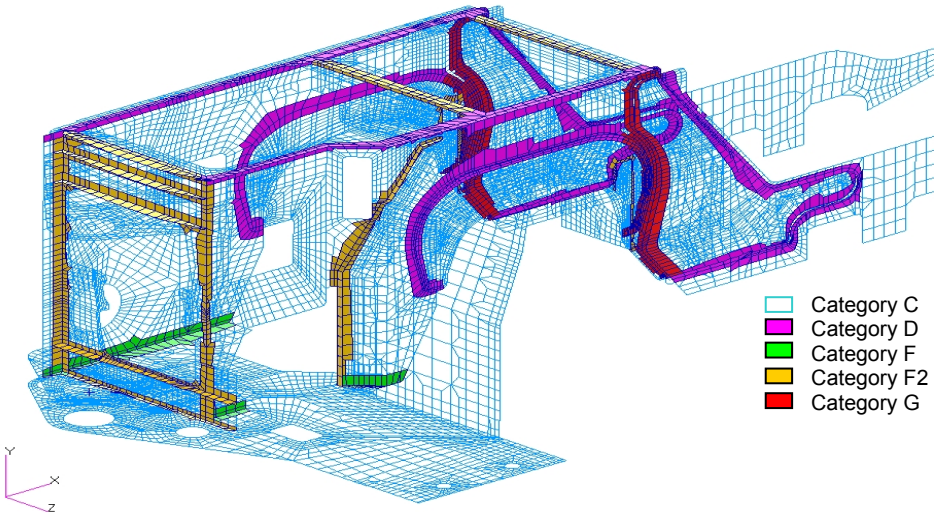

Figure 6-14 Weld categories according to BS7608

Using MSC FATIGUE solver, the stress results from the load factors as discussed in paragraph 5.4.6.3 were used to calculate the damage for the whole finite element model, using different S-N curves for each category. The result of this analysis would be the damage of one cycle for the whole model for each load case. The damages for the three load cases can then be summed, and then inversed again to give the number of cycles the structure will survive for the combined load case. As mentioned in paragraph 5.4.6.2, 2 million of these cycles corresponds to a life of 10000 hours. The result of this analysis is depicted in Figure 6-15.

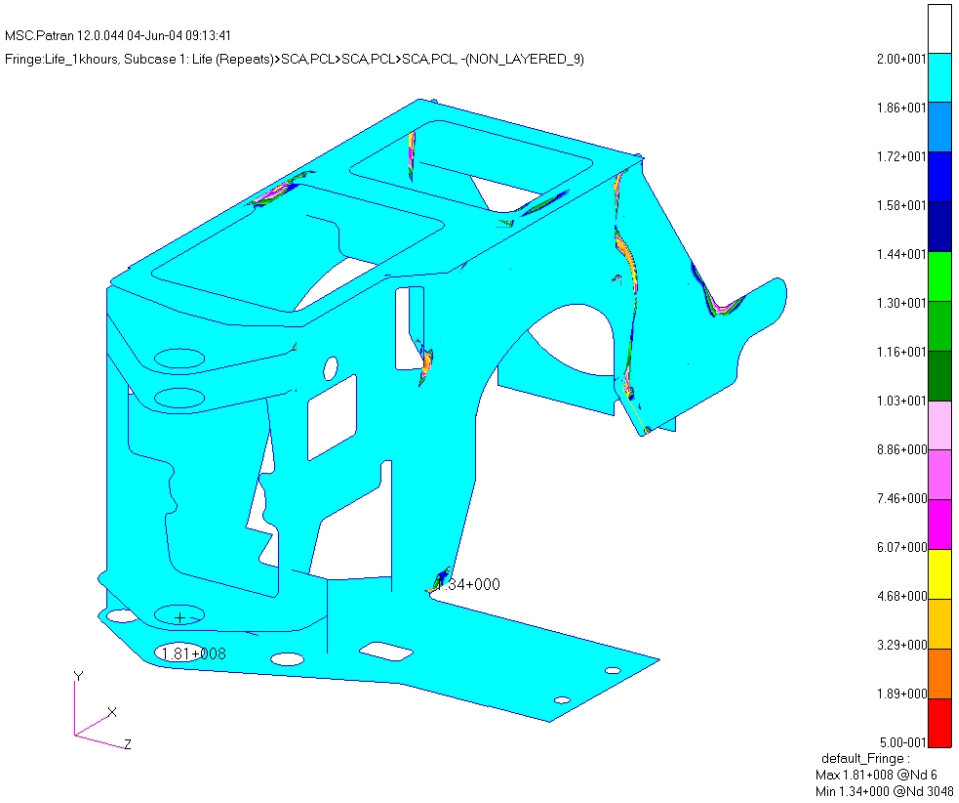

Figure 6-15 Fatigue life results for LHD

6.2.6.2 Correlation with field failures

Cracks were found on the chassis of a vehicle that was approximately 6 000 hours old. Photographs of these cracks, together with the corresponding fatigue life prediction contour plots, are depicted in Figure 6-16. Adequate correlation is achieved.

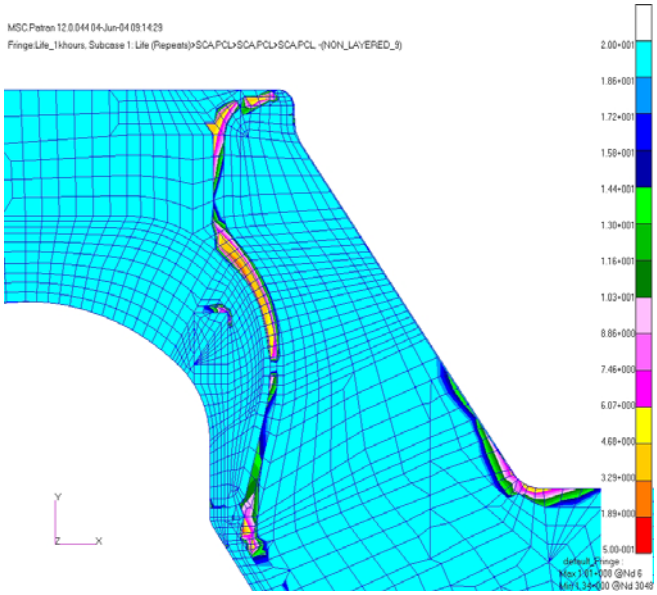

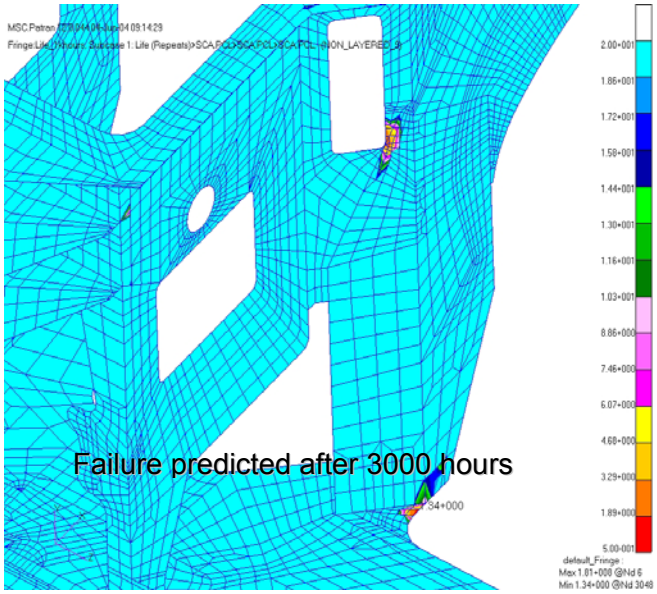

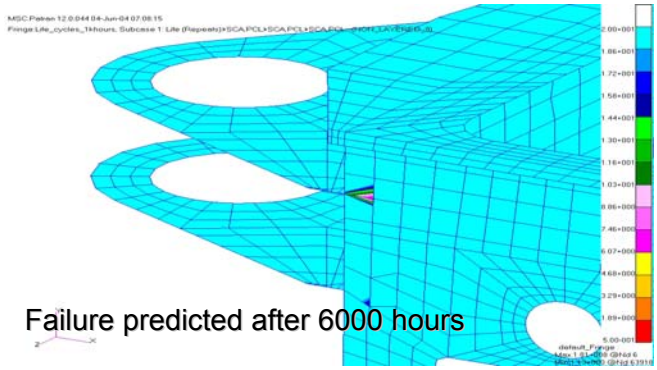

Figure 6-16 Correlation of predicted failures and field failures for LHD

6.3 DESIGN CODE CORRELATION

6.3.1 General

Comparisons of the input loads derived for the fuel tanker and the ISO tank container to relevant design codes, are performed in this section.

6.3.2 Fuel Tanker

6.3.2.1 Types of stresses calculated

South African fuel tankers are required by law to comply to two South African Bureau of Standards codes, namely:

- SABS (South African Bureau of Standards) 1398. (1994). *Road tank vehicles for petroleum based flammable liquids.*
- SABS (South African Bureau of Standards) 1518. (1996). *Transportation of dangerous goods – design requirements for road tankers.*

Both codes require the calculation of maximum principal stresses to be assessed against the allowable stresses. Any specific point at any position on the structure could be subjected to a combination of normal stresses (tensile or compressive in three possible directions) and shear stresses (also in three possible directions). At the surface (where maximum stresses always occur due to bending and torsion), the normal stress perpendicular to the surface, as well as the two shear stresses in the surface plane, must be zero, leaving two normal stresses and one shear stress to be determined. The maximum principal stress would be a normal stress caused by a combination of these three stresses in some principal direction in the plane of the surface.

During the finite element analysis, maximum principal stresses, TRESCA stresses, as well as sometimes Von Mises stresses, were calculated. The latter two types of stresses are basically equivalent. They differ from maximum principal stresses by virtue of the fact that they are equal to the difference between the maximum and the minimum principal stresses. They were calculated for the following reasons:

- The fatigue, as well as the yielding failure mechanism, are in fact driven by these stresses, rather than by maximum principal stresses.
- These stresses will always be equal or larger than the maximum principal stress on the surface, since one principal stress will always be zero and the maximum principal stress minus zero (if no negative principal stress exists) will be equal to the maximum principal stress. These stresses therefore yield more conservative (but necessarily so) results.

The calculated TRESCA or Von Mises stresses were therefore regarded as maximum principal stresses for the purpose of the codes.

A further interpretation required for assessing the calculated stresses in terms of the SABS codes, concerns the difference between local and global stresses. Both SABS codes are intended for simplified calculations of stresses on mostly cylindrical type tank vessels. Global bending, tensile and shear stresses are calculated by considering the vessel as a beam. When performing a detailed finite element analysis, especially on a complex geometry such as the fuel tanker structure, some very localised stresses are calculated at stress concentration positions. The allowable global stress criteria of the

codes are then inappropriate (sometimes being conservative or unconservative) and a more detailed assessment using BS 8118 (1991), is invoked.

6.3.2.2 SABS 1398

Acceleration forces are to be applied as separate load cases to the fully loaded vehicle. These are:

- 2 g longitudinal
- 2 g vertical
- 1 g lateral

For each of these load cases, the maximum allowable principal stresses in the tank wall are required to be lower than 20 % of the tensile strength of the material.

6.3.2.3 SABS 1518:1996

This code requires a combination of acceleration forces for load conditions expected during normal use. Additional to this, accident loads must be investigated according to other criteria. For normal use the design load requirements are:

- 0.75 g longitudinal + 1.7 g vertical + 0.4 g lateral

and the maximum allowable principal stresses must be less than 25% of the ultimate tensile strength of the material.

Design loads in the event of an accident are:

- 2 g longitudinal

and stress levels (maximum principal) must be less than 75% of the yield strength of the material.

6.3.2.4 BS 8118 (FESL)

BS 8118 does not specifically apply to tanker vehicles, but is a general structural design code for aluminium, which deals with static as well as dynamic loading conditions. For the limit state static design, the BS 8118 code requires the following loading.

Maximum expected loading factored by load factor (γ_f = 1.33):

- 0.75 g x 1.33 longitudinal + 1.7 g x 1.33 vertical + 0.4 g x 1.33 lateral

The resultant stresses should then be less than the factored resistance of the material (γ_m = 1.3), with material resistances given for the raw material, the heat affected raw material, the welding material, as well as the heat affected zone (HAZ) material. For dynamic loading, the BS code gives material properties for different details. The equivalent fatigue loading used is derived in paragraph 5.4.4.3.

6.3.2.5 Comparison of codes

Table 6-4 below gives a comparison of the different codes. If only regarding the vertical loading, the different codes compare as follows in terms of allowable stresses for the extrusions for 1 g vertical loading:

- SABS 1398: 28 MPa
- SABS 1518: 41 MPa
- BS 8118 static: 50 MPa (for HAZ)
- BS 8118 fatigue + FESL: 32 MPa (for weld class 20)

It is demonstrated that the FESL criterion derived for the fuel tanker, combined with BS 8118, is similar to the requirements of the SABS codes. The FESL method, however, has the benefit that it accounts explicitly for fatigue and differentiates between different fatigue strength categories in the design (for class 20 and higher categories, SABS 1398 would become progressively more conservative, but it would become unconservative for classes lower than 20.

Table 6-4 Comparison of different fuel tanker design code requirements

	SABS 1398	SABS 1518	BS 8118 Static	BS 8118 Fatigue
Longitudinal	2 g	0.75 g (2 g)	1 g	
Vertical	2 g	1.7 g	2.26 g	0.62 g
Lateral	1 g	0.4 g	0.53 g	
	Separate	Combined	Combined	
Allowable stress plates	62 MPa	77.5 MPa (232.5 MPa)	181 MPa for raw material 188 MPa for weld material 115 MPa for HAZ material	Typ. > 35 MPa for raw material Typ > 20 MPa for weld material (depending on classification)
Allowable stress extru.	56 MPa	70 MPa	185 MPa for raw material 146 MPa for weld material 112 MPa for HAZ material	

6.4 DERIVATION OF USAGE PROFILE FROM FIELD FAILURE DATA

6.4.1 General

Field failure data could be the most valuable source from which usage profiles may be derived. Goes (1995) argues that good or bad experiences of the ultimate tester, the customer, rarely find their way into the new product.

The successful mathematical model developed for failure prediction in paragraph 6.2.2 above prompted an attempt to develop a reverse method from which the two-parameter statistical usage profile could be derived by using only the available failure data, without the questionnaire and measurement data. This methodology is demonstrated based on the minibus case study.

6.4.2 Methodology

6.4.2.1 Probability density function

The bivariate lognormal PDF (Eq. 5.24), which defines the statistical usage profile, has five unknown constants:

- Mean of y_1 (μ_{y1})
- Mean of y_2 (μ_{y2})
- Standard deviation of y_1 (σ_{y1})
- Standard deviation of y_2 (σ_{y2})
- Correlation coefficient (ρ)

Ranges of interest for these parameters may be estimated. It is firstly assumed that the relative damage calculations are such scaled that the damage to failure for the structure/component for which failure statistics are known, is unity (i.e. $D_f = 1$).
Distances travelled before failure occurs could range from 10 000 km to 10 000 000 km, implying a total range for x_1 of D_f / distance = 1/10000 to 1/10000000 and for $y_1 = \ln(x_1)$ = -9.2 to –16.1. It is conceivable that one standard deviation in terms of distance to failure

may imply a maximum factor of 10 on the distance, or σ_{y1} = ln(10) = 2.3. Applying a standard deviation of 2.3 to the total range of y_1, it may then be argued that the range for the mean of y_1 could be estimated as μ_{y1} = -16.1 +2.3 = -13.8 to –9.2 –2.3 = -11.5.

Similarly, it may be estimated that x_2 for a population of vehicle owners may vary from 100 to 30 000 km/month (rather than km/day), implying y_2 = ln(x_2) = 4.6 to 10.3. Applying again a standard deviation of σ_{y2} = 2.3, the range for the mean of y_2 could be estimated as μ_{y2} = 4.6+2.3 = 6.9 to 10.3-2.3 = 8. These calculations are summarised in Table 6-5.

Table 6-5: Ranges of parameters

	Total min	-Max std dev	+Max std dev	Total max
Distance to failure	10000	100000	1000000	10000000
x1=1/Distance to failure	1.00E-04	1.00E-05	1.00E-06	1.00E-07
y1	-9.2	-11.5	-13.8	-16.1
x2=distance per month	100	1000	3000	30000
y2	4.6	6.9	8.0	10.3

The correlation coefficient (ρ) could vary between 0 (no correlation between two parameters y_1 and y_2) and –1 (full inverse proportionality). In practice, values between –0.1 and –0.5 would be expected, since some correlation would always exist (less distance on rough roads), but certainly not full proportionality. A typical set of values would therefore be:

μ_{y1} = -12.6 μ_{y2} = 7.5
σ_{y1} = 1 σ_{y2} = 1
ρ = -0.3

The bivariate Probability Density Function for these parameters is depicted in Figure 6-17. A contour plot of the PDF is depicted in Figure 6-18.

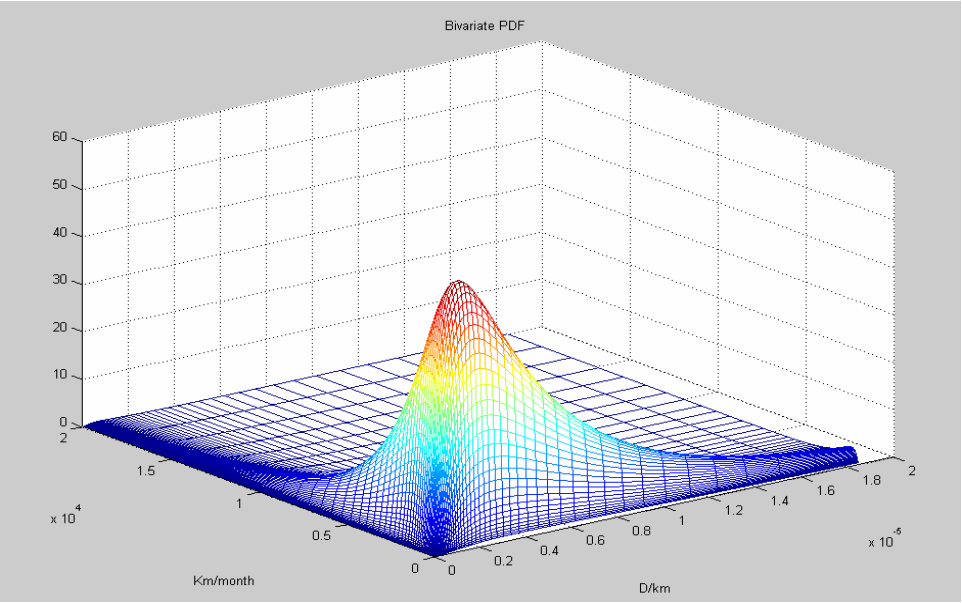

Figure 6-17: Probability Density Function for typical parameters

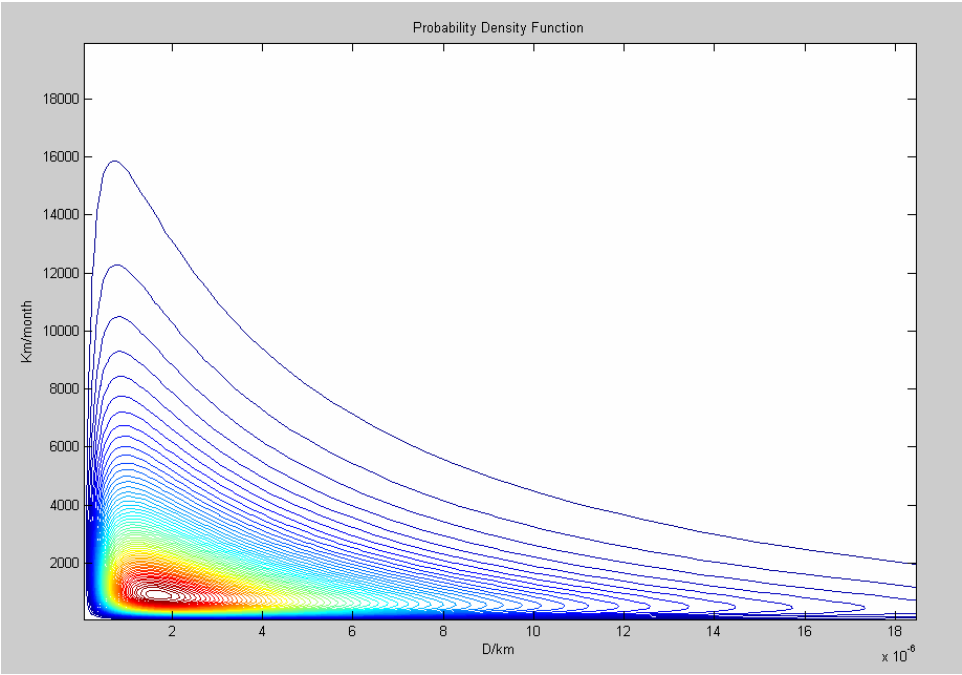

Figure 6-18: Contour plot of PDF for typical parameters

Plotting the PDF on a logarithmic scale for both axes (using the natural logarithm), yields a bivariate normal distribution, as depicted in Figure 6-19. On the same plot, the constant damage per time period (in this case, D = 1 and period = 12 months) lines, which are hyperbolas on a linear scale plot (see Figure 6-1), is depicted. The probability of a vehicle that is 12 months old, exceeding a damage of D = 1, can be calculated as the volume of the PDF to the right and above the 12 month line (the shaded area).

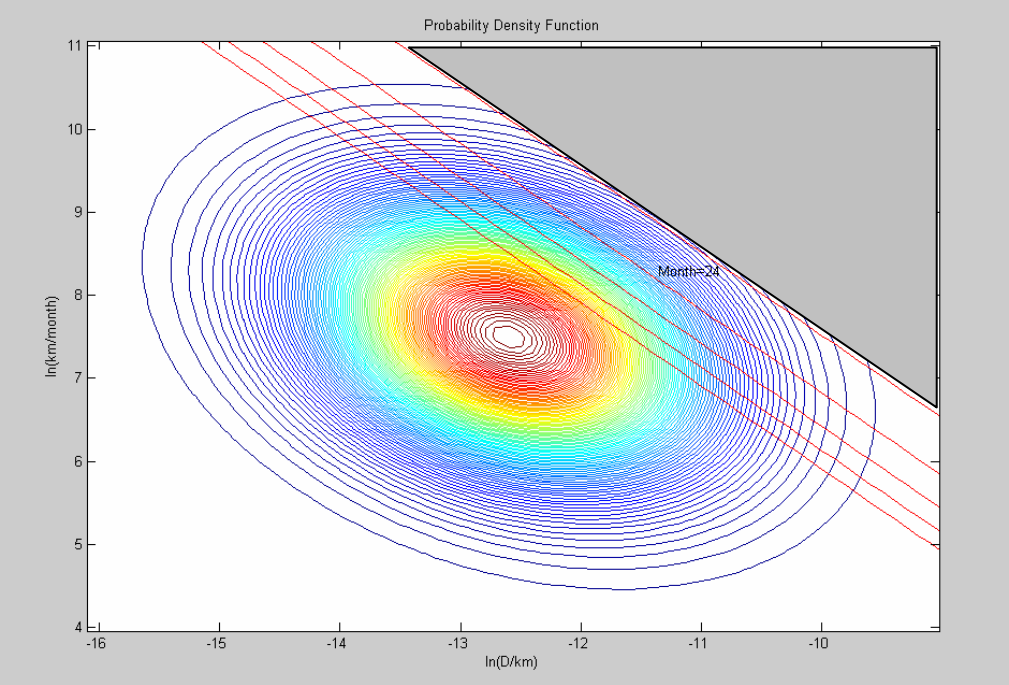

Figure 6-19: Contour plot of PDF for typical parameters on logarithmic scales

6.4.2.2 Failure data

Normally for any vehicle, available failure data would include the distance travelled by the failed vehicle, as well as its age. After performing a fatigue test to reproduce the experienced failure, the relative damage (D_f) to produce failure (with a known relation to cycles on the test track), would also be known. It is therefore possible to calculate the values of both parameters (dam/km and km/month) for each incidence of failure:

$$D/km = D_f / (\text{distance to failure})$$

$$km/month = (\text{distance to failure}) / (\text{age in months})$$

A Monte Carlo simulation method for predicting failures, depicted in Figure 6-20, was implemented as MATLAB code, in order to have a software tool to produce a simulated set of the above failure statistics for a given set of usage profile parameters.

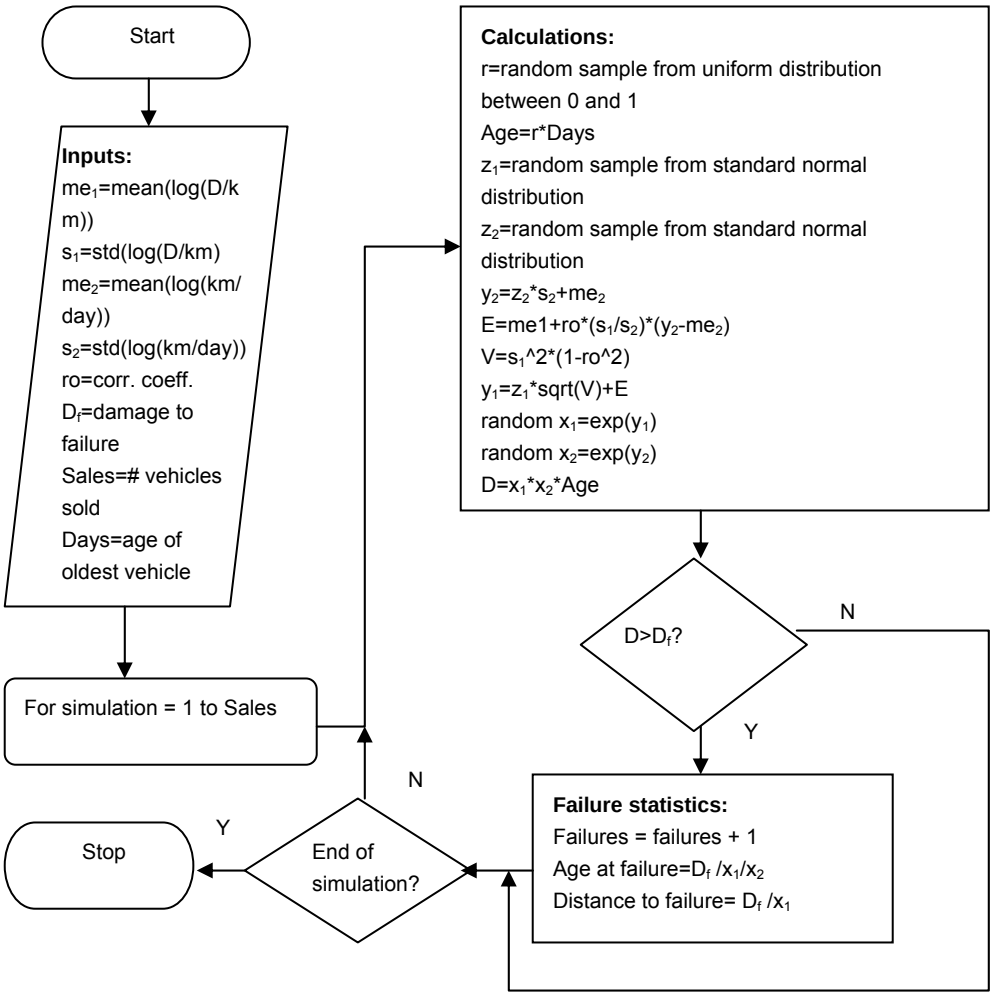

Figure 6-20: Monte Carlo simulation method

In all cases, it was assumed that the relative fatigue damages are scaled such that D_f = 1. The simulation was performed for a period of 5 years (60 months), with an assumed uniform sales distribution of 100 vehicles per month.

The first simulation was performed for the typical usage profile parameters listed above. 484 failures were simulated out of the total population of 6 000 vehicle (8 %). Figure 6-

21 depicts the contours of the PDF, the constant damage/month lines, as well as the failure parameters (D/km and km/month). Each failure incidence is represented by a star.

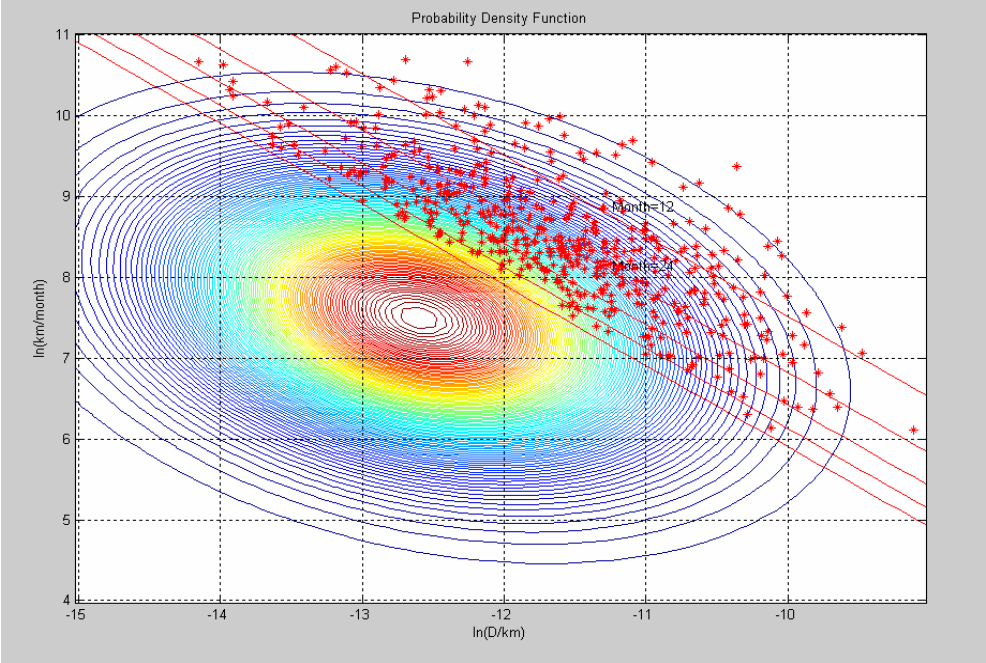

Figure 6-21: PDF contours and failure parameters

It is obvious that all failures would fall above the 60-month line (all vehicles are younger than 60 months), but it can be observed that the density of failures also exhibits some correlation with the contours of the PDF.

Although the failure parameters represent a sample of the total population, it is a particularly biased sample and can therefore not be used directly to estimate the means and standard deviations for the total population. The parameter values represent failed vehicles and should therefore be expected to be on the tails of the distributions.

The failure prediction method involves a complex process and a pure mathematical reversal cannot be achieved. However, based on the visible correlation between the density of the failures and the PDF contours, it was decided to develop a curve fitting technique to estimate usage profile parameters from failure statistics.

6.4.2.3 Curve fitting

The failure incidences are firstly binned into bins of constant ln(km/month) and ln(D/km) increments. The coarseness of these increments depends on the number of failures. These results are then normalised with respect to the exposure of each bin. Bins falling between two subsequent constant damage/month lines (e.g. between the lines of D/month = 1/50 and 1/51) could be populated with failed vehicles of any age older than 50 months, implying an exposure to a total number of 10 months (60 months – 50 months) multiplied by 100 vehicles sold per month = 1000 vehicles. The failure rate of each bin would therefore be proportional to the number of failures recorded in that bin, divided by 1000. Bins falling between the next set of lines (i.e. between the lines of D/month = 1/49 and 1/50) could be populated with failed vehicles of any age older than 49 months, implying an exposure to a total number of 11 months (60 months – 49 months) multiplied by 100 vehicles sold per month = 1100 vehicles.

The failures counted in each bin are therefore divided by the number of vehicles that could make up that count. The resultant value of each bin should then be proportional to the PDF value at the coordinates of the bin, since this PDF value is proportional to the number of vehicles out of a total population that would have the parameters of the bin.

The result of this exercise for the simulated failures is depicted in Figure 6-22.

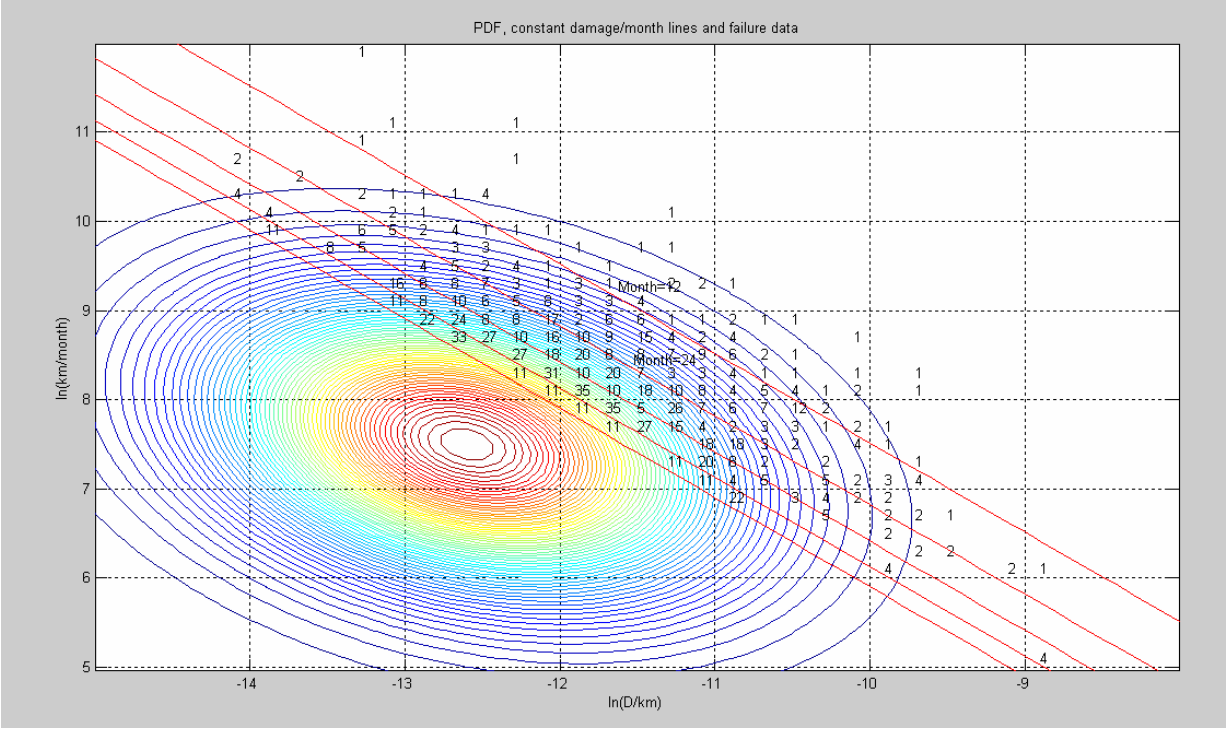

Figure 6-22 PDF contours with binned & normalised failure numbers

It is therefore argued that the binned and normalised failure values depicted in Figure 6-22, when multiplied by an unknown scale factor (K), would approximately fall on the PDF surface. The problem of estimating the usage profile parameters from failure data therefore reduces to curve fitting the PDF, divided by K, onto the set of binned and normalised failure values.

Mathematically, the problem is defined as follows:

> Solve the non-linear curve-fitting problem in the least-squares sense, that is, given input data xdata and output ydata, find coefficients P that "best-fit" the equation F(P, xdata), i.e.;
>
> $$\min_{x} \tfrac{1}{2}\left\|F(P,xdata)-ydata\right\|_2^2 = \tfrac{1}{2}\sum_i \left(F(P,xdata_i)-ydata_i\right)^2$$
>
> where,
>
> xdata = coordinates (ln(D/km),ln(km/month)) of the bins
> ydata = the normalised failure values of the bins
> F = PDF (defined by Eq. 4) / K
> P = unknown parameters (μ_{y1}, μ_{y2}, σ_{y1}, σ_{y2}, ρ, K)

Eq. 6-6

MATLAB provides a built-in function "lsqcurvefit", which uses the large-scale algorithm to solve the above problem. This algorithm is a subspace trust region method and is based on the interior-reflective Newton method described by Coleman and Li (1994), (1996). The values for (μ_{y1}, μ_{y2}, σ_{y1}, σ_{y2} and ρ), calculated from the failure data, together with an arbitrary K, are used as initial values of P, to commence the iterations. The values listed in Table 6-5 are used to bind the parameters.

Using this algorithm and the failure data depicted in Figure 6-22, the following result was obtained:

	μ_{y1}	μ_{y2}	σ_{y1}	σ_{y2}	ρ
True values	-12.6	7.5	1	1	-0.3
Curve fit results	-12.27	8	1.13	1.05	-0.5

These results are graphically represented in Figure 6-23. The accuracy of the curve fitted result is considered to be adequate. Using the estimated parameters to predict failures during the 5-year period, results in a failure percentage of 15 % instead of the 'true' 8 %, which would be an acceptable prediction, given the accuracy and cost of alternative prediction methods.

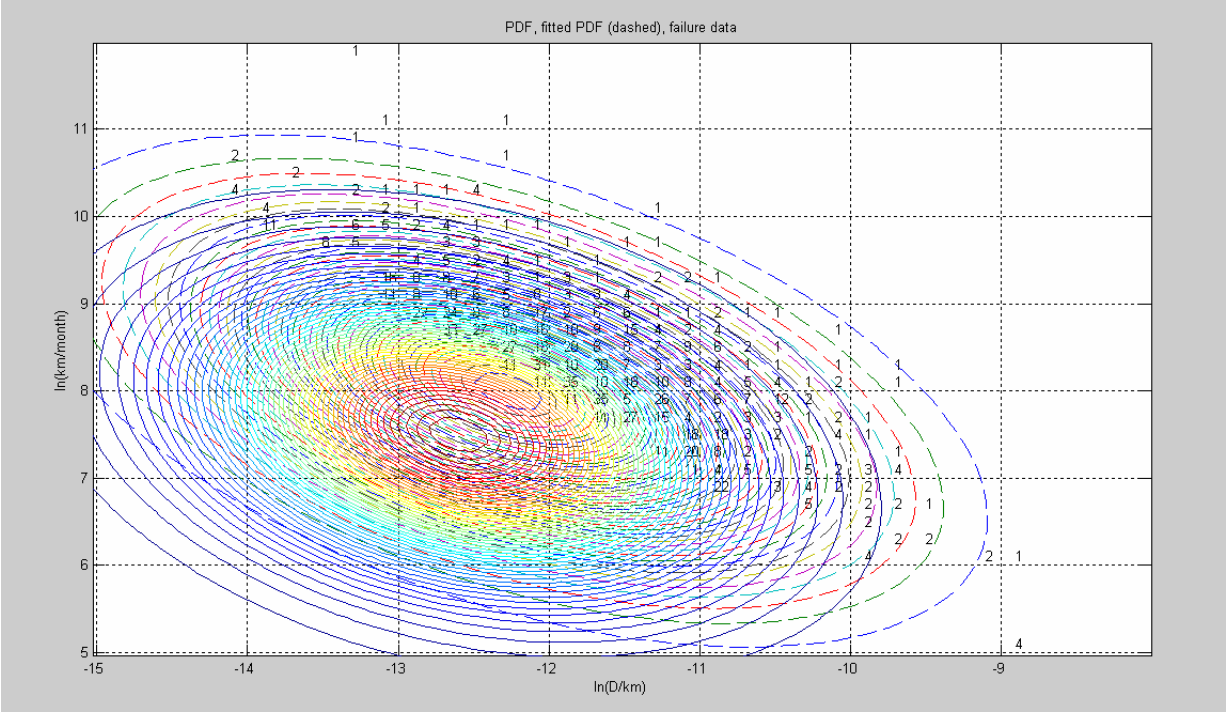

Figure 6-23 PDF of typical values, curve fitted PDF & failure data

Several more trials were performed to test the method. In each case a random set of usage profile parameters were generated (within the boundaries discussed before). These values were used to perform the Monte Carlo simulation to produce failure statistics. The curve-fitting algorithm was then applied to the normalised failure data. The results of these trials are presented in graphical and tabular form below.

	μ_{y1}	μ_{y2}	σ_{y1}	σ_{y2}	ρ
True values	-13.25	7.28	0.36	1.37	-0.26
Curve fit results	-13.07	7.76	0.46	1.41	-0.5

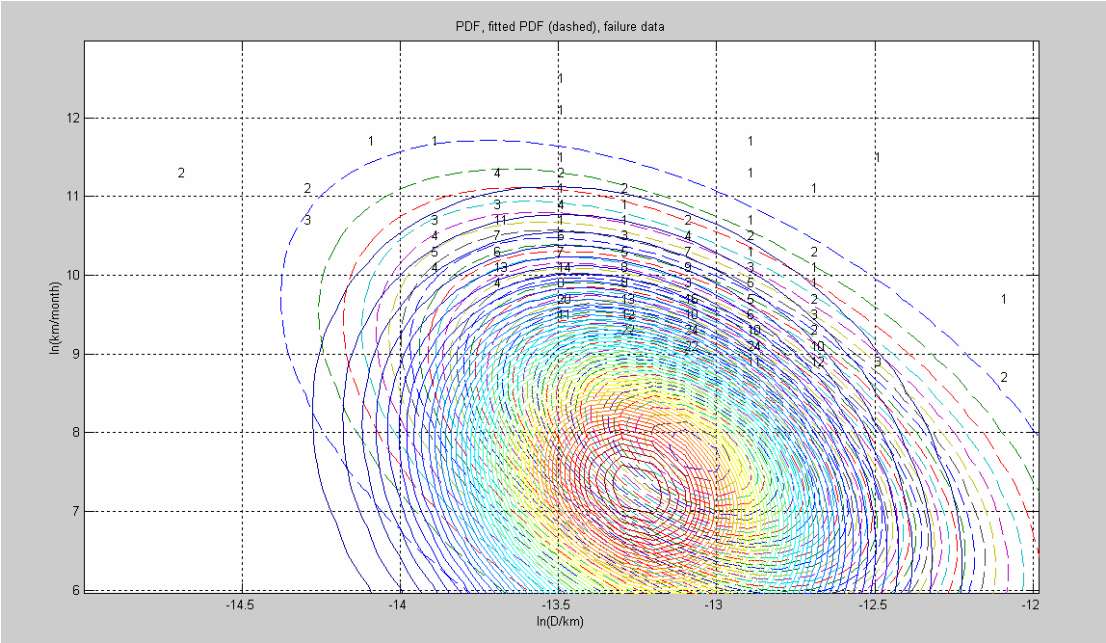

Figure 6-24 Case A – 3 % failures

	μ_{y1}	μ_{y2}	σ_{y1}	σ_{y2}	ρ
True values	-12.28	7.17	0.78	1.83	-0.11
Curve fit results	-12.43	6.9	0.89	1.89	-0.1

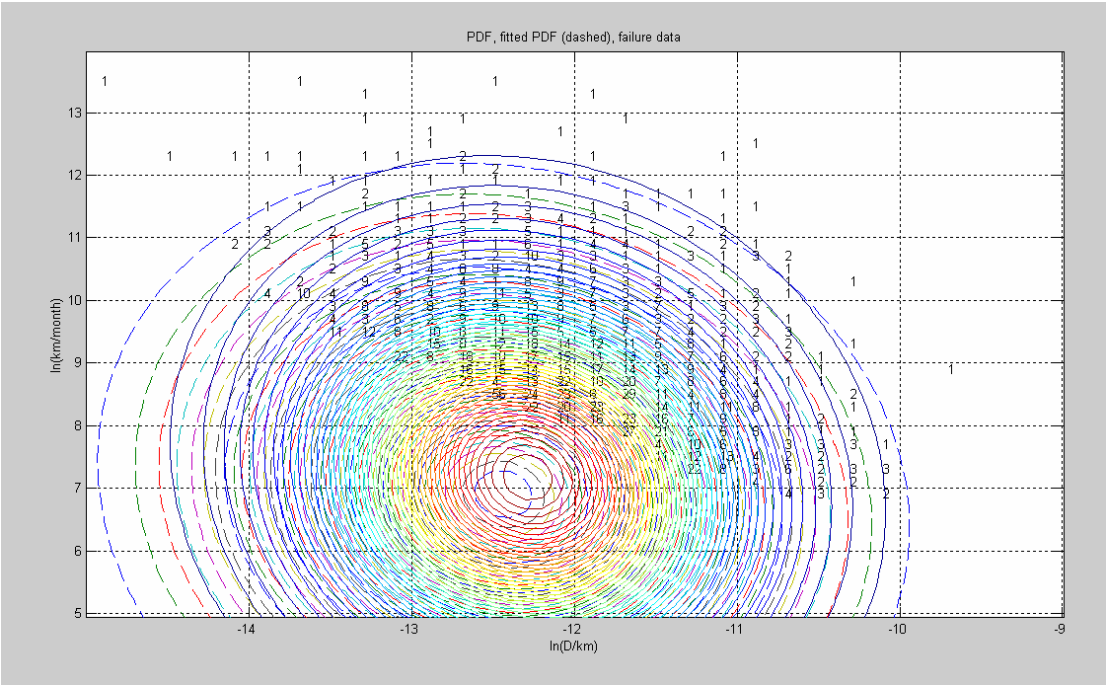

Figure 6-25 Case B – 16 % failures

	μ_{y1}	μ_{y2}	σ_{y1}	σ_{y2}	ρ
True values	-13.5	7.0	0.8	0.8	-0.2
Curve fit results	-13.8	6.9	1.16	1.18	-0.46

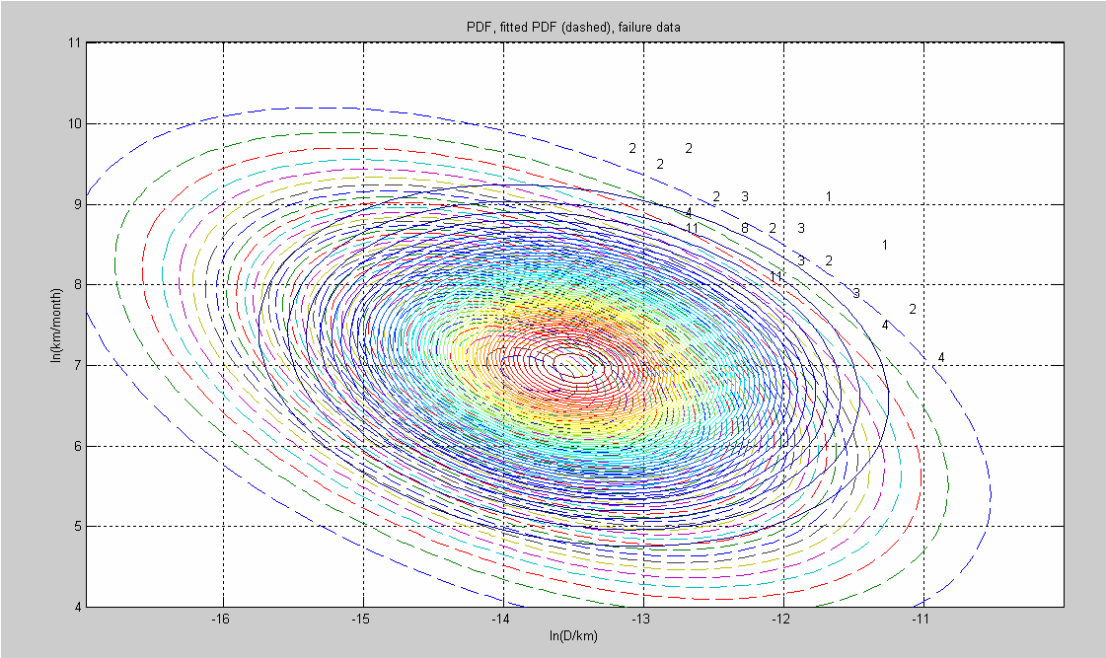

Figure 6-26 Case C – 0.4 % failures

It is clear from the above trials that the accuracy improves for higher failure percentages, which is to be expected. It is however argued that the method would still be useful for failure percentages as low as 0.5 %.

A methodology was presented that would enable vehicle designers to derive a statistical fatigue loading profile of the total population of users of a vehicle model from failure data recorded on the same or a previous model. The method is radically more economic than existing methods and entails a few hours of running a software program, together with performing a failure test on the component for which failure data is available to determine the damage to failure. It was demonstrated that reasonable accuracy could be achieved, even if the failures represent only a small fraction of the total population. The two-parameter usage profile thus determined can powerfully be used to predict failures or derive statistically based durability test or design requirements.